

Anti-HER2 immunoliposomes for selective delivery of electron paramagnetic resonance imaging probes to HER2-overexpressing breast tumor cells

Scott R. Burks · Luciana F. Macedo · Eugene D. Barth · Katherine H. Tkaczuk · Stuart S. Martin · Gerald M. Rosen · Howard J. Halpern · Angela M. Brodie · Joseph P. Y. Kao

Received: 2 November 2009 / Accepted: 23 December 2009
© Springer Science+Business Media, LLC. 2010

Abstract Electron paramagnetic resonance (EPR) imaging is an emerging modality that can detect and localize paramagnetic molecular probes (so-called spin probes) in vivo. We previously demonstrated that nitroxide spin probes can be encapsulated in liposomes at concentrations exceeding 100 mM, at which nitroxides exhibit a concentration-dependent quenching of their EPR signal that is analogous to the self-quenching of fluorescent molecules. Therefore, intact liposomes encapsulating high concentrations of nitroxides exhibit greatly attenuated EPR spectral signals, and endocytosis of such liposomes represents a cell-activated contrast-generating mechanism. After

endocytosis, the encapsulated nitroxide is liberated and becomes greatly diluted in the intracellular milieu. This dequenches the nitroxides to generate a robust intracellular EPR signal. It is therefore possible to deliver a high concentration of nitroxides to cells while minimizing background signal from unendocytosed liposomes. We report here that intracellular EPR signal can be selectively generated in a specific cell type by exploiting its expression of Human Epidermal Growth Factor Receptor 2 (HER2). When targeted by anti-HER2 immunoliposomes encapsulating quenched nitroxides, Hc7 cells, which are novel HER2-overexpressing cells derived from the MCF7 breast tumor cell line, endocytose the liposomes copiously, in contrast to the parent MCF7 cells or control CV1 cells, which do not express HER2. HER2-dependent liposomal delivery enables Hc7 cells to accumulate 750 μ M nitroxide

Electronic supplementary material The online version of this article (doi:10.1007/s10549-009-0715-4) contains supplementary material, which is available to authorized users.

S. R. Burks · G. M. Rosen · J. P. Y. Kao (✉)
Medical Biotechnology Center, University of Maryland
Biotechnology Institute, 725 W. Lombard St., Baltimore, MD
21201, USA
e-mail: jkao@umaryland.edu

S. R. Burks · G. M. Rosen · J. P. Y. Kao
Center for Biomedical Engineering and Technology, University
of Maryland, Baltimore, MD 21201, USA

S. R. Burks · G. M. Rosen · J. P. Y. Kao
Center for EPR Imaging In Vivo Physiology, University
of Maryland, Baltimore, MD 21201, USA

K. H. Tkaczuk · S. S. Martin · A. M. Brodie
Marlene and Stewart Greenebaum Cancer Center, University
of Maryland, Baltimore, MD 21201, USA

S. R. Burks · S. S. Martin · J. P. Y. Kao
Department of Physiology, University of Maryland, Baltimore,
MD 21201, USA

L. F. Macedo · A. M. Brodie
Department of Pharmacology, University of Maryland,
Baltimore, MD 21201, USA

K. H. Tkaczuk
Department of Medicine, University of Maryland, Baltimore,
MD 21201, USA

G. M. Rosen
Department of Pharmaceutical Sciences, University
of Maryland, Baltimore, MD 21201, USA

E. D. Barth · H. J. Halpern
Department of Radiation Oncology and Center for EPR Imaging
In Vivo Physiology, University of Chicago, Chicago, IL 60657,
USA

intracellularly. Through the use of phantom models, we verify that this concentration of nitroxides is more than sufficient for EPR imaging, thus laying the foundation for using EPR imaging to visualize HER2-overexpressing Hc7 tumors in animals.

Keywords Electron paramagnetic resonance spectroscopy · Imaging · Breast cancer · HER2 · Liposomes · Nitroxides

Introduction

Detecting micrometastatic breast tumor lesions remains a persistent challenge for current imaging methods, but one that has clear clinical implications. Even when current detection methods reveal no clinical evidence of metastasis, disseminated tumor cells can be found in the bloodstream and bone marrow of 60% of breast cancer patients [1]. In 32% of patients whose lymph nodes were scored negative by routine histopathology, serial sectioning and immunohistochemistry nonetheless revealed micrometastases [2]. Such disseminated and micrometastatic tumor cells predict poor patient survival [1, 2], but tend to divide slowly; therefore, they can be highly resistant to conventional chemotherapy [3]. The ability to detect micrometastases and monitor their response to therapies could be significantly improved by imaging methods that can be targeted to specific characteristics of the tumor cell with increased resolution and sensitivity.

Very-low-frequency electron paramagnetic resonance imaging (EPRI) is an attractive emerging modality for imaging metastatic breast tumor lesions. EPRI can detect and image paramagnetic species *in vivo* and in real time [4]. Endogenous paramagnetic molecules are too scarce to be detected by EPRI; therefore, exogenous “spin probes” such as nitroxides must be used to label features of interest. EPRI using nitroxides offers several advantages. First, the radiofrequency waves used to excite resonance penetrate tissues well, enabling deep-tissue imaging with high signal-to-noise ratio (SNR) and high spatial resolution. Second, the magnetic moment of the electron, which is imaged by EPRI, is ~660-fold greater than that of the proton [5]. This makes EPRI potentially more sensitive than proton magnetic resonance imaging (MRI). Third, spin probes can be designed to be sensitive to cellular physiology; therefore, in addition to localizing a tumor, they can also report on its physiology. Physiological parameters that can be measured with spin probes include tissue oxygen tension [6, 7], microviscosity [8], pH [9], temperature [10], and redox status [11].

We previously synthesized nitroxides that are well retained by cells and thus exhibit long-lived intracellular

signals that can be imaged by EPRI [12, 13]. We have also shown that nitroxides, like fluorophores, when encapsulated in liposomes at high concentrations (>100 mM), show concentration-dependent signal quenching. Thus, intact liposomes containing quenched probes are spectroscopically invisible. After endocytosis by cells, however, lysis of the liposomes liberates and dilutes the encapsulated probes into the cell; the resulting dequenching of the probe signal renders the cell visible [14]. Encapsulation of probes at high concentration minimizes background signal from unendocytosed liposomes and creates a cell-activated contrast-generating mechanism. By itself, however, liposomal delivery is limited by the inability to deliver probe molecules selectively to a particular cell type.

As a tool for delivering imaging agents to a physiologically distinct tissue such as a breast tumor, liposomes must be targetable, *i.e.*, they must incorporate features that enable selective uptake in a tissue of interest, but not in other, indifferent, tissues. Liposomal surfaces can be readily decorated with moieties that target them to a specific tissue. For example, immunoliposomes, bearing surface-conjugated antibody fragments, can target distinct antigens. Specifically, immunoliposomes targeted against the human epidermal growth factor receptor 2 (HER2) have been used to enhance delivery of chemotherapeutics to HER2-expressing tumors [15, 16].

HER2 is a receptor-tyrosine-kinase in the *erbB* family [17]. It is overexpressed in some breast, ovarian, and non-small-cell lung cancers [18]. Approximately 30% of primary breast tumors have HER2 overexpression [19, 20], which is associated with cell proliferation, tumor progression [21], and poor clinical prognosis [20]. Therefore, HER2 is an important target for diagnostics and therapeutics. One major therapeutic advance has been the development of humanized monoclonal antibodies against HER2 (*e.g.*, trastuzumab). Trastuzumab binds the extracellular domain of HER2 and inhibits tumor progression through several mechanisms. Binding of HER2 by trastuzumab potentially inhibits receptor heterodimerization, which is required for RTK signaling [22]; it also induces HER2 internalization, which limits receptor activation [23–25].

While trastuzumab has therapeutic activity, it has garnered attention as a targeting agent for HER2. The receptor-mediated endocytosis of HER2 consequent to therapeutic antibody binding makes trastuzumab an ideal targeting agent for delivering xenobiotics to HER2-expressing cells. Antibody-mediated targeting of HER2 has been used to deliver different imaging diagnostics to HER2-overexpressing tumor cells. The approaches generally involve attaching imaging probes directly to the antibody, including near-infrared fluorophores for *in vivo* optical imaging [26], radionuclides for positron emission

tomography [27], and superparamagnetic iron oxide for MRI [28]. In view of these developments, we surmised that EPRI probes could be delivered to HER2-overexpressing breast tumor cells by anti-HER2 immunoliposomes.

Immunoliposomes are an attractive alternative to delivery approaches in which “cargo” molecules are conjugated directly to the antibody. Such approaches deliver only a few molecules per antibody, and are therefore not efficient for imaging applications, where large numbers of probe molecules must be delivered to maximize imageable signal. Immunoliposomes encapsulating high concentrations of nitroxides can deliver large quantities of molecular probes upon endocytosis by the targeted cell, while contributing minimal background signal in circulation.

We have generated a stable HER2-overexpressing cell line, Hc7, from MCF7 human breast tumor cells. Hc7 cells express high levels of HER2 at the cell surface, and are thus well suited for immunoliposomal targeting studies. We demonstrate in two ways that immunoliposomes bearing trastuzumab Fab' fragments target Hc7 cells with high specificity. First, HER2-targeting immunoliposomes encapsulating quenched fluorophores generate intense intracellular fluorescence after endocytosis by Hc7 cells, but not in cells that have little or no HER2 expression. Second, Hc7 cells endocytose nitroxide-loaded immunoliposomes and accumulate sufficient intracellular nitroxide to enable EPRI with high contrast. This work lays the foundation for using EPRI to visualize and investigate HER2-overexpressing tumors in animals.

Materials and methods

General materials and methods

Dipotassium (2,2,5,5-tetramethylpyrrolidin-1-oxyl-3-ylmethyl)amine-*N,N*-diacetate (nitroxide **1**, Fig. 1) was synthesized as described previously [12]. 6-Carboxyfluorescein (CF) and 3-carboxy-2,2,5,5-tetramethyl-1-pyrrolidinyloxy (nitroxide **2**, Fig. 1) from Sigma (St. Louis, MO) were converted to the corresponding potassium salts by adding stoichiometric equivalents of KOH. Lipids were from Avanti Polar Lipids (Alabaster, AL); cell culture media and biochemicals were from Life Technologies (Grand Island, NY) or Sigma; chromatography resins were from Pharmacia (Piscataway, NJ) or GE Healthcare (Piscataway, NJ). A multilabel counter (Wallac Victor² 1420-015; Perkin-Elmer, Waltham, MA) was used for protein assays: protein content was measured by absorbance at 595 nm [5 μ l diluted 50-fold into premixed Coomassie Brilliant Blue G-250 (Sigma)]; sulfhydryl groups were determined by absorbance at 412 nm (in 0.004% w/v 5,5'-dithio-bis-(2-nitrobenzoic acid)). Data analyses and presentation were performed with

Origin 8.0 (OriginLabs, Northampton, MA), Photoshop CS3 (Adobe Corp., San Jose, CA), Matlab 2009a (The Mathworks, Natick, MA), and Volocity 5.1 (Improvision, Waltham, MA). One-way ANOVA was used to determine differences among data sets; $P < 0.05$ was considered significant. Bonferroni tests were used for post hoc analysis.

Cell culture

CV1 cells (American Type Culture Collection, Manassas, VA) and MCF7 cells (gift from Richard J. Santen, University of Virginia) were maintained at 37°C under 5% CO₂, in Dulbecco's Modified Eagle Medium (DMEM) supplemented with 10% (v/v) fetal bovine serum (FBS), 2 mM L-glutamine, and Pen/Strep (100 U/ml penicillin, 100 μ g/ml streptomycin). Hc7 cells were cultured identically but with supplementation of 500 μ g/ml hygromycin B. For microscopy, all cells were cultured on 25-mm round No. 1 glass coverslips for 24–48 h.

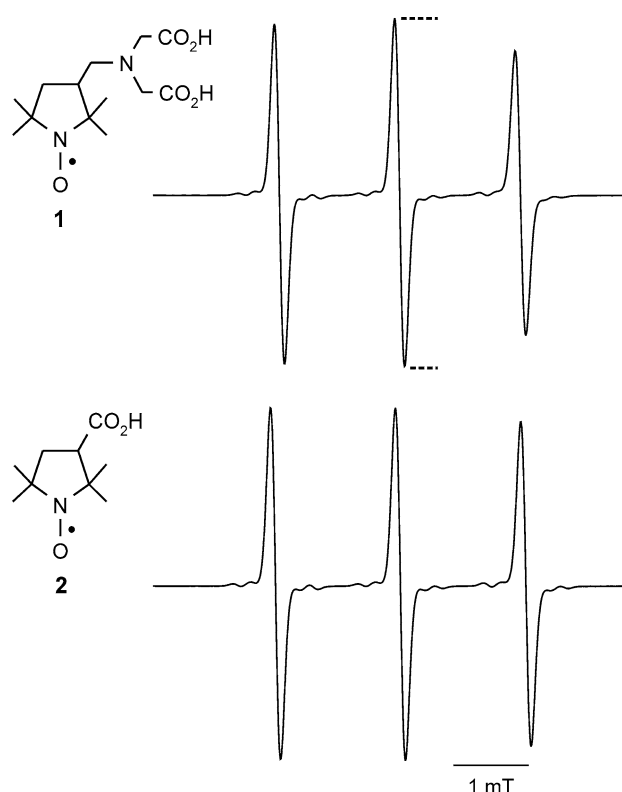


Fig. 1 Structures and EPR spectra of nitroxides. The structures of nitroxides **1** and **2** are shown at left. The corresponding 3-line EPR spectra, acquired at the same nitroxide concentration, are shown at right (experimental details in “Materials and methods”). Reported EPR spectral intensity is the height of the center peak, as indicated by the dotted lines

Derivation of Hc7 cells that stably overexpress HER2

To a 10-fold dilution of Fugene-6 (Roche, Indianapolis, IN) in serum- and antibiotic-free DMEM, pcDNA3.1 vector incorporating HER2 cDNA and a hygromycin selection marker (gift from Dr. Anne Hamburger, University of Maryland, Baltimore) was added (39 $\mu\text{g}/\text{ml}$) and incubated for 30 min; 100 μl of this mixture were added to 8 ml of FBS-containing antibiotic-free DMEM and used to transfect 2×10^5 MCF7 cells plated on 60-mm plastic Petri dishes. After 24 h, the medium was replaced with fresh DMEM containing FBS and Pen/Strep. At 96 h post-transfection, hygromycin B (500 $\mu\text{g}/\text{ml}$) was added. Antibiotic-resistant colonies were isolated and passaged more than ten times prior to analysis for HER2 overexpression.

Western immunoblotting

Hc7 cells were lysed in radio-immunoprecipitation assay buffer. Total protein (50 μg) was resolved by SDS-PAGE under reducing conditions. Proteins were transferred to Hybond-ECL membranes (Biorad, Hercules, CA) and probed with rabbit-anti-human antibodies against phospho-HER2 and β -actin (Millipore, Billerica, MA). Secondary hybridization with horseradish peroxidase (HRP)-conjugated, anti-rabbit antibodies was visualized with an enhanced chemiluminescence kit (Biorad).

Trastuzumab Fab' fragments for immunoliposomes and immunostaining

Trastuzumab (10 mg, 8 mg/ml in 20 mM Na acetate, pH 4.5) was added to 125 μl of immobilized pepsin gel (Pierce, Rockford, IL) which had been washed three times in the same buffer. Digestion (37°C, 4 h) yielded F(ab')₂ fragments and was stopped by raising the pH to 6.5 with 1 M Tris; the pepsin gel was removed by centrifugation.

Reduction with 50 mM cysteamine for 45 min at 37°C converted the F(ab')₂ fragments into Fab' fragments. The reaction mixture was chromatographed on Sephadex G-15 equilibrated with elution buffer [100 mM NaCl, 50 mM Na citrate (pH 6.7), 2 mM EDTA] that was purged with N₂ for 30 min. During elution, the buffer reservoir was sparged with N₂. Fractions containing Fab' were collected under N₂, immediately frozen in liquid N₂, and stored at -80°C until used for making immunoliposomes.

For immunofluorescence experiments, Fab' fragments were incubated with maleimide (20 mM, 4°C, 8 h) under N₂ to block free sulfhydryl groups. The maleimide-modified Fab' fragments were eluted from Sephadex G-15 with Dulbecco's Phosphate Buffered Saline (DPBS).

HER2 immunostaining

MCF7, CV1, and Hc7 cells were fixed with 4% paraformaldehyde in DPBS (pH 7.4) for 20 min. All steps were at room temperature; each step was followed by three washes with DBPS. Nonspecific antigen sites were blocked with 10% (v/v) normal rabbit serum in DBPS for 1 h. Cells were incubated for 3 h in DPBS with the following primary antibodies: trastuzumab IgG, 1 $\mu\text{g}/\text{ml}$; maleimide-inactivated trastuzumab Fab', 0.38 $\mu\text{g}/\text{ml}$. The secondary antibody was fluorescein isothiocyanate (FITC)-conjugated, Fab-specific, rabbit anti-human IgG (3 $\mu\text{g}/\text{ml}$ in DPBS; Jackson ImmunoResearch, West Grove, PA). Secondary hybridization was for 1 h in the dark. Labeled cells were maintained in DPBS for fluorescence microscopy.

Immunoliposome preparation

Liposomes were composed of 1,2-distearoylphosphatidylcholine (DSPC), cholesterol (Chol), ammonium *N*-(lissamine rhodamine B sulfonyl)-1,2-dipalmitoylphosphatidylethanolamine (Rhod-PE), and ammonium 1,2-distearoyl-*sn*-glycero-3-phosphatidylethanolamine-*N*-[maleimide-poly(ethyleneglycol)2000] (PE-PEG-maleimide) in the molar ratio 3 DSPC:2 Chol:0.06 PE-PEG-maleimide:0.003 Rhod-PE. 10–30 μmol of phospholipid in 100 μl EtOH were injected into 0.5 ml of a rapidly stirred aqueous solution of 100 mM CF or 150 mM nitroxide 1. The mixture was passed eleven times through a 100-nm porosity filter membrane in a Mini Extruder (Avanti Polar Lipids) to yield a suspension of liposomes. The extruder and all solutions were maintained at >55°C to ensure fluidity of the lipid phase. Liposomes were purified on Sephadex G-50 with the same anaerobic buffer used to purify Fab' fragments. Freshly prepared liposomes were incubated with Fab' fragments under N₂ (4°C, overnight). The immunoliposomes were purified on Sephacryl HR-200 with DPBS as eluant and stored at 4°C. Antibody coupling was verified by SDS-PAGE (Supplemental Fig. S1); nitroxide retention was verified by EPR spectroscopy (Supplemental Fig. S2).

Cellular uptake of CF-loaded immunoliposomes

Rhod-PE-containing immunoliposomes encapsulating 100 mM CF were used as a suspension in Hanks' Balanced Salt Solution (HBSS) at a concentration of 0.025 μmol phospholipid/ml. Hc7, MCF7, or CV1 cells were incubated with 2 ml of liposome suspension at 37°C for 4 h. After three brief washes with Ca²⁺- and Mg²⁺-free HBSS containing 1 mM EDTA, the cells were maintained in normal HBSS for fluorescence microscopy.

Cellular uptake of nitroxide-loaded immunoliposomes

Hc7 cells in replicate 60-mm plastic Petri dishes were incubated at 37°C with Rhod-PE-containing immunoliposomes (2 ml, 0.025 μmol phospholipid/ml in HBSS) encapsulating 150 mM nitroxide **1**. At various times, cells were washed with HBSS, released from the plate with trypsin–EDTA, and centrifuged at 145×*g* for 3 min; the resulting pellet was washed twice with Ca²⁺- and Mg²⁺-free HBSS containing 1 mM EDTA. The cells were resuspended in 400 μl normal HBSS, lysed with 120 μM digitonin, and sonicated for 1 min. Cell-associated nitroxide and Rhod-PE were analyzed spectroscopically. Nitroxide concentration in each sample was determined using a standard curve of EPR spectral intensity versus nitroxide concentration. Average cell count per dish was determined by counting control dishes; total intracellular volume was calculated using a measured volume of 2.5×10^{-12} l/cell (Supplemental Fig. S3). The average intracellular nitroxide concentration was then estimated through volumetric calculations.

EPR spectroscopy

EPR spectra were acquired using a quartz flat-cell in an X-band spectrometer (E-109, Varian, Palo Alto, CA) at the following settings: microwave power, 20 mW; frequency, 9.55 GHz; field center, 333.5 mT; modulation amplitude, 0.05 mT; modulation frequency, 100 kHz; time constant, 0.5 s. The magnetic field was scanned from 0.8 to 8 mT at 2.67 mT/min. Data acquisition was through EWIN software (Scientific Software Services, Plymouth MI). Reported spectral intensity is the amplitude of the center peak in the nitroxide triplet spectrum (Fig. 1).

Fluorescence spectroscopy

Fluorescence spectra were recorded on a spectrofluorometer (model CM1T-10I, SPEX Industries, Metuchen, NJ) controlled through Datamax software (Galactic Industries, Salem, NH). Excitation and emission wavelengths for Rhod-PE were 550 and 588 nm, respectively.

Fluorescence microscopy

An inverted microscope (TE200, Nikon, Tokyo, Japan) equipped with a ×40 oil-immersion objective (Super Fluor, NA 1.4) was used for fluorescence microscopy. A monochromator (PolyChrome II, TILL Photonics, Gräfelfing, Germany) supplied excitation light. Fluorescence was bandpass-filtered before capture by a CCD camera (CoolSnap HQ, Roper Scientific, Tucson, AZ). Instrument

control, image acquisition, and analysis were performed with MetaFluor software (Molecular Devices, Downingtown, PA).

EPR imaging, image reconstruction, and analysis

A nitroxide-impregnated agarose phantom was prepared by boiling a 4% (w/v) agarose solution, then adding 100 μM nitroxide **2** and drawing the solution into a serological pipette (6-mm i.d.). The agarose was then sectioned into 3-mm-long cylinders. The cylinder was molded in polyvinylsiloxane dental impression material (GC Dental Products, Kasugai, Japan) and centered in the resonant cavity of a 250-MHz EPR imaging spectrometer [4] fitted with a loop-gap resonator (with single loop and single gap). The sample-holding loop (19-mm diameter, 15-mm depth) had a loaded Q of 172. A 0.55-mT spectral window encompassed the central peak of the nitroxide spectrum. Instrumental parameters were: RF power, 12 dB; modulation amplitude and frequency, 0.198 mT and 4.98 kHz, respectively; lock-in time constant, 100 ms, with 100-ms-per-point dwell time; 64 points per projection; field gradient, 48.9 mT/m. Signal intensity in the EPR image is proportional to nitroxide EPR signal. Under identical conditions, nitroxides **1** and **2** show essentially identical EPR spectral signals (see Fig. 1); therefore commercially available nitroxide **2** was adequate for use in the phantom.

Continuous-wave (CW) EPR images were obtained using an essentially tomographic technique. Projections are defined as field-scanned CW spectra in the presence of a 48.9-mT/m gradient. Each scan, comprising 64 points uniformly spaced in the magnetic field, was obtained in 6.4 s; each projection was the average of four scans. Sixty-six projections were acquired at 10 polar angles; multiple azimuthal angles were sampled at each polar angle. A filtered back-projection algorithm was used for image reconstruction [29]. Projections were filtered using a simple cutoff of the image response frequency to half the Nyquist sampling limit.

Spatial resolution of an imaging system is commonly defined by the full-width-at-half-maximum (FWHM) of a point spread function (PSF). For a phantom cylinder of known dimensions, the FWHM can be estimated from the edge profile of signal intensity [30]. A two-dimensional cross section from the reconstructed image, taken through the center of the cylinder and orthogonal to the axis, was analyzed. Twenty intensity profiles uniformly spaced around the circumference of the cylinder were analyzed to yield an average FWHM of 4.4 ± 0.4 mm. To determine SNR, the mean signal intensity in a region-of-interest (ROI) containing signal was ratioed against the standard deviation of the noise in an identically sized ROI containing only noise.

Results

Hc7 cells express high levels of HER2 at the plasma membrane

MCF7 breast tumor cells were stably transfected to overexpress HER2. HER2 expression in the resulting Hc7 transfectants were analyzed by western blot (Fig. 2). The blot confirms that when compared to MCF7 cells, Hc7 cells have much higher HER2 expression, but provides no information regarding subcellular HER2 localization. Because immunoliposomes can only target receptors that are accessible extracellularly, it is important to verify that HER2 is highly expressed at the cell surface. Hc7, MCF7, and CV1 cells were fixed with paraformaldehyde but without detergents, immunostained with trastuzumab IgG as the primary antibody and a FITC-conjugated, Fab-specific secondary antibody, and analyzed by fluorescence microscopy (Fig. 3). CV1 cells, which are African Green Monkey kidney epithelial cells, do not express the exclusively human HER2 receptor, and were used as the control for nonspecific labeling. As shown in Fig. 3a, Hc7 cells express HER2 abundantly at the cell surface, whereas untransfected MCF7 cells show only very feeble HER2 expression. As the quantitative summary in Fig. 3b shows, immunofluorescence in Hc7 cells was much greater than in MCF7 and in the negative-control CV1 cells (ANOVA $F_{2,36} = 75.97$).

Trastuzumab Fab' fragments retain antigen-binding ability

Intact trastuzumab avidly binds HER2, but the antibody must be proteolyzed and reduced to generate Fab' fragments that can be conjugated to liposomes. To assess the antigen-binding affinity and selectivity of the Fab' fragments, Hc7, MCF7, and CV1 cells were immunostained as outlined above, with the exception that primary antibodies

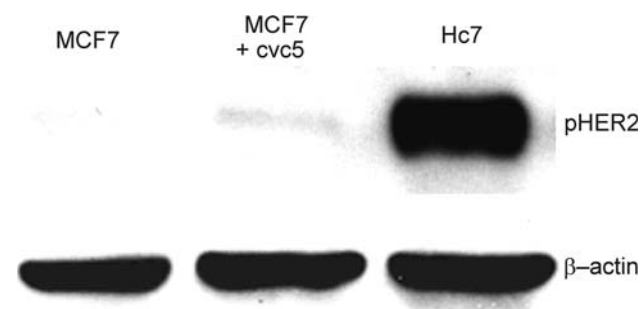


Fig. 2 Western blots for HER2. *Top row:* Hc7 cell lysates show high expression of phospho-HER2 when compared to untransfected MCF7 cells or MCF7 cells transfected with the *cvc5* vector, which lacks HER2 DNA. *Bottom row:* β -actin staining as loading control

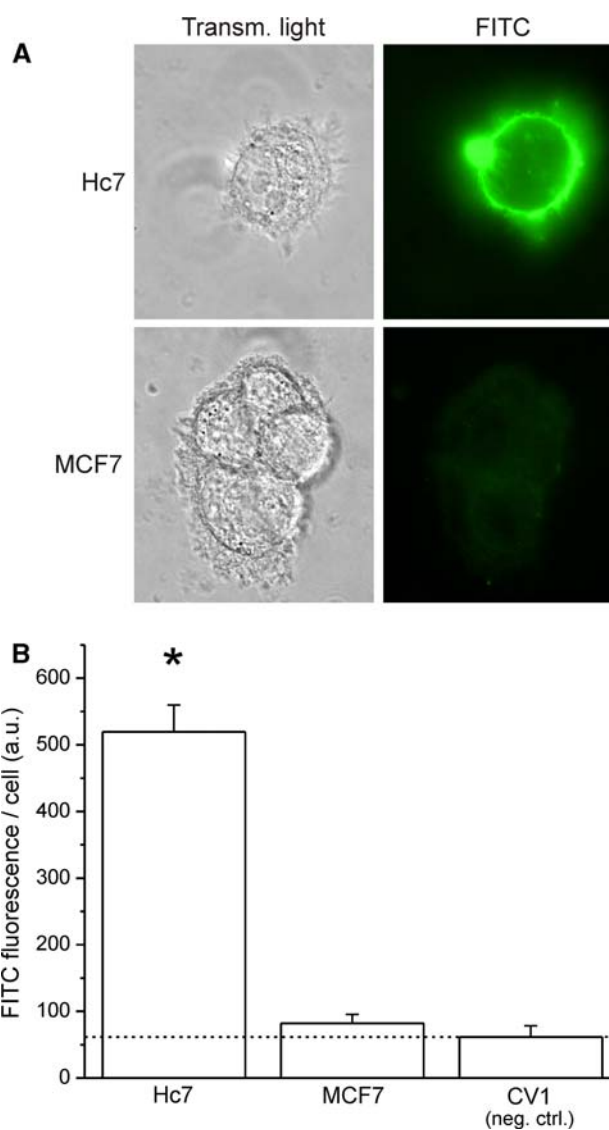


Fig. 3 Immunostaining for plasma-membrane-localized HER2. Cells were fixed with paraformaldehyde (pH 7.4) in the absence of detergents. Trastuzumab IgG was used as the primary antibody, with a human-Fab-specific, FITC-conjugated secondary antibody. **a** Representative transmitted-light and fluorescence images of Hc7 and MCF7 cells after immunofluorescence staining. **b** Quantitation of average FITC fluorescence per cell for three cell lines: Hc7, which overexpresses HER2; MCF7, which expresses physiological levels of HER2 and, as negative control, CV1, which has no HER2 expression (*dotted line* indicates the fluorescence of the CV1 negative control; *error bars* represent SEM; ANOVA: $F_{2,36} = 75.97$)

were Fab' fragments whose exposed reactive thiol groups had been inactivated with maleimide (Fig. 4). Immunofluorescence was again much greater in Hc7 cells than in MCF7 and in negative-control CV1 cells (ANOVA $F_{2,38} = 31.38$). Moreover, when ANOVA is performed on the combined data from Figs. 3b and 4b, post hoc analysis reveals that in each cell line, regardless of whether the intact IgG or the Fab' fragment was used as the primary

antibody, no significant difference in FITC fluorescence was observed. However, when comparing Hc7 and MCF7 cells, FITC fluorescence was always significantly higher in Hc7 cells irrespective of which primary antibody was used (ANOVA $F_{5,75} = 37.28$). Therefore, trastuzumab Fab' fragments bind HER2 as avidly and selectively as intact trastuzumab IgG, and should allow immunoliposomes to target the receptor.

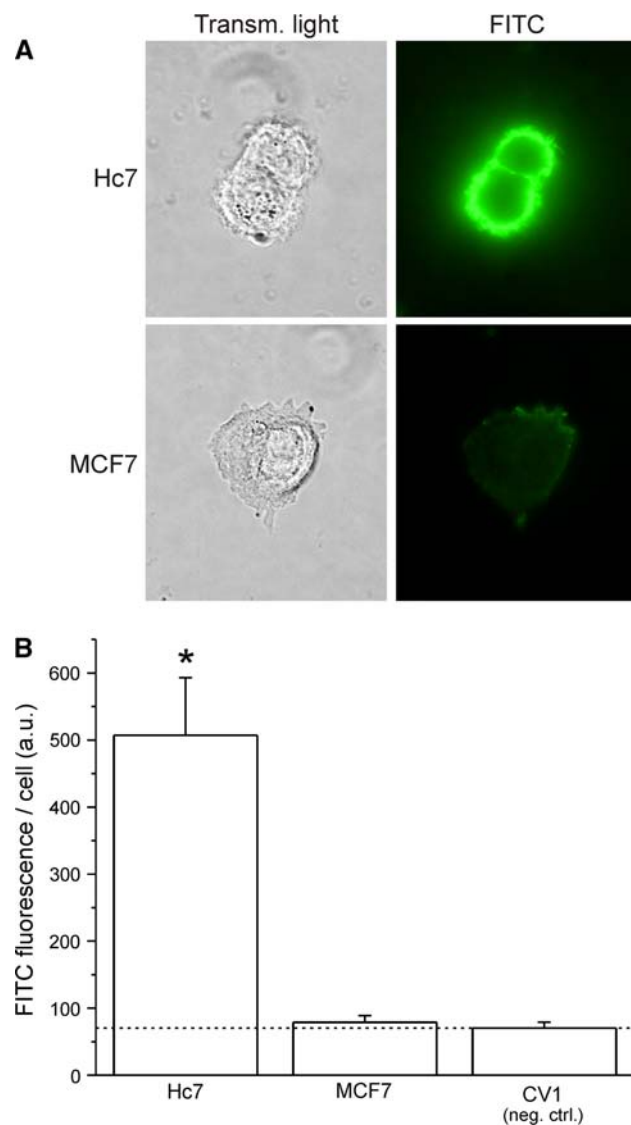


Fig. 4 Trastuzumab Fab' fragments retain immunoreactivity with HER2. Primary staining was done with maleimide-inactivated trastuzumab Fab' fragments using the same protocol in Fig. 2. **a** Representative transmitted-light and fluorescence images of Hc7 and MCF7 cells after immunofluorescence staining. **b** Quantitation of average FITC fluorescence per cell for three cell lines: Hc7, which overexpresses HER2; MCF7, which expresses physiological levels of HER2 and, as negative control, CV1, which has no HER2 expression (dotted line indicates the fluorescence of the CV1 negative control; error bars represent SEM; ANOVA: $F_{2,38} = 31.38$)

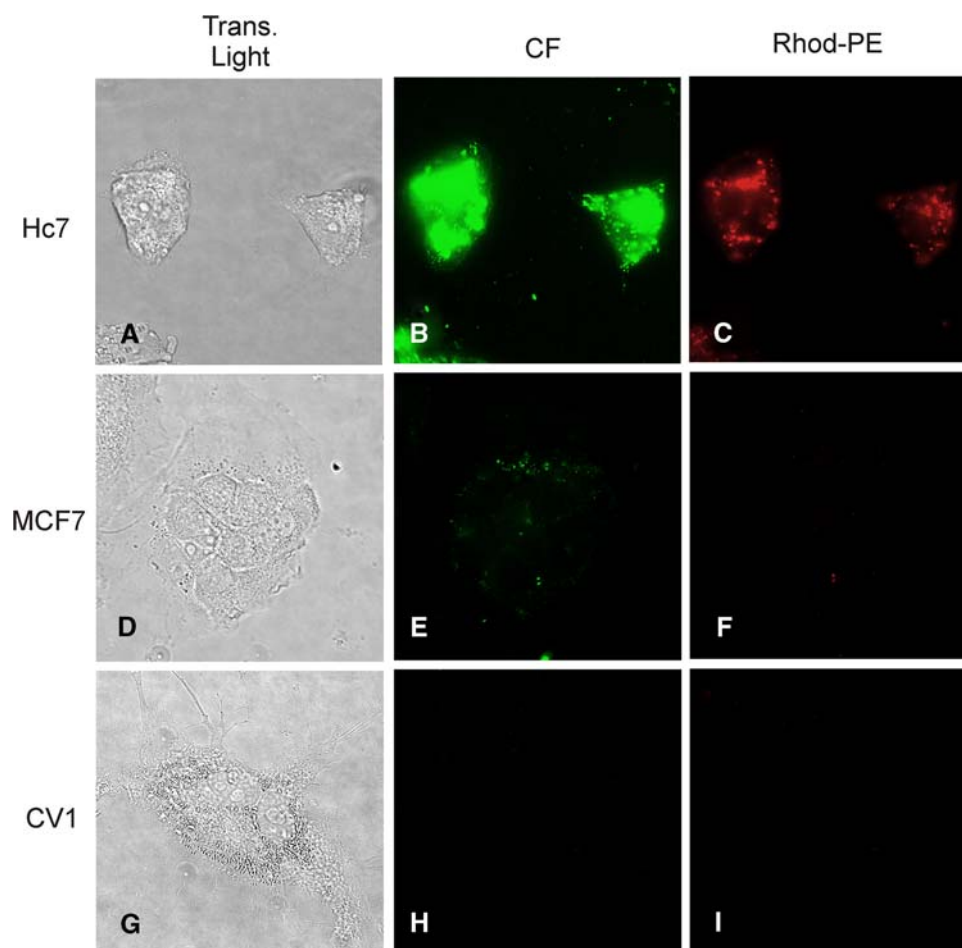
Immunoliposomal delivery of fluorescent probes generates intense intracellular fluorescence in HER2-overexpressing cells

Hc7, MCF7, or CV1 cells were incubated for 4 h with anti-HER2 immunoliposomes incorporating Rhod-PE and encapsulating 100 mM CF, rinsed with Ca^{2+} - and Mg^{2+} -free, EDTA-containing HBSS, and then maintained in normal HBSS for fluorescence imaging (Fig. 5). As shown in Fig. 5 (panels a–c), Hc7 cells exhibit bright intracellular CF fluorescence (green) as the result of immunoliposome internalization and subsequent release and dequenching of the encapsulated CF. The Hc7 cells also show intense, more spatially nonuniform, intracellular Rhod-PE fluorescence (red), which is indicative of incorporation of Rhod-PE lipid from the immunoliposomes into intracellular membranes. In contrast, MCF7 cells, which express only physiological levels of HER2, endocytose few immunoliposomes and thus show very feeble intracellular CF and Rhod-PE fluorescence (Fig. 5, panels d–f). Lastly, CV1 cells, which do not express HER2, have no detectable fluorescence signals (Fig. 5, panels g–i). These results indicate that endocytic uptake of immunoliposomes is dependent on HER2 expression, and that it is possible to generate intense intracellular signals selectively in HER2-overexpressing breast tumor cells.

Hc7 cells achieve high intracellular nitroxide concentrations through endocytosis of immunoliposomes

Replicate dishes of Hc7 cells were incubated with immunoliposomes incorporating Rhod-PE, and encapsulating 150 mM nitroxide **1**. At various times, cells were trypsinized and washed with Ca^{2+} - and Mg^{2+} -free, EDTA-containing PBS. The amount of nitroxide and Rhod-PE associated with the cells was determined spectroscopically as described in “Materials and methods”. Cell-associated nitroxide and Rhod-PE initially increased in parallel with time of incubation (Fig. 6), as expected from endocytic uptake of liposomes and their luminal contents. At 6 h, cell-associated nitroxide peaked at $\sim 750 \mu\text{M}$. By 9 h, intracellular nitroxide concentration had declined to $\sim 350 \mu\text{M}$, whereas cell-associated Rhod-PE was unchanged from the level observed at 6 h. This suggests that beyond 6 h, endocytosis became very slow. Without continued uptake of liposomes for replenishment, cellular transport processes that extrude nitroxides [12] dominated, leading to a net loss of intracellular nitroxide signal. Even so, intracellular nitroxide concentrations were in the several hundred micromolar range.

Fig. 5 Incubation with anti-HER2 immunoliposomes containing Rhod-PE and encapsulating carboxyfluorescein (CF) generates bright intracellular signals in Hc7 cells, but not MCF7 or CV1 cells. Panels **a**, **d**, and **g** are transmitted light images; panels **b**, **e**, and **h** show fluorescence in the fluorescein channel; panels **c**, **f**, and **i** show fluorescence in the rhodamine channel. HER2-overexpressing Hc7 cells (**a–c**) avidly endocytose immunoliposomes, as evidenced by the intense red fluorescence of Rhod-PE (**c**). Endocytosis results in dequenching of CF to generate bright intracellular green fluorescence (**b**). MCF7 cells (**d–f**) express a physiological level of HER2 and endocytose fewer liposomes, giving rise to only feeble fluorescence. CV1 cells (**g–i**), which express no HER2, exhibit no fluorescence



Agarose phantom containing 100 μM nitroxide can be visualized by EPRI with high contrast

To investigate the possibility of imaging Hc7 cells that have selectively accumulated nitroxides through endocytosis of immunoliposomes, we constructed an EPR imaging phantom consisting of an agarose cylinder impregnated with 100 μM nitroxide **2**. The phantom was readily imaged by EPRI (Fig. 7) with a SNR of 79. The known geometry of the cylinder is well represented in the EPR image, which has a spatial resolution of 4.4 ± 0.4 mm. These findings indicate that if immunoliposomal delivery could cause Hc7 cells in vivo to accumulate nitroxide at concentrations comparable to those observed in vitro (Fig. 6), then Hc7 tumors can be easily imaged by EPRI.

Discussion

We have demonstrated that anti-HER2 immunoliposomes encapsulating quenched fluorophores and nitroxides can be targeted to, and generate robust spectral signals in, Hc7 cells, which overexpress HER2. This study, by showing that

immunoliposomes enable cell-activated contrast generation only in the targeted cell type, significantly enhances the utility of our earlier finding that endocytosis of liposomes can serve as a cell-activated contrast-generating mechanism [14],

For this study we generated a new cell line, Hc7, from the MCF7 breast tumor line. Hc7 cells overexpress HER2 at the cell surface and thus can be targeted by anti-HER2 immunoliposomes. Immunofluorescence showed that the HER2 expression level in Hc7 cells is comparable to what has been observed in other HER2-overexpressing tumor lines such as A431 or BT-474 [31]. Anti-HER2 immunoliposomes encapsulating CF are avidly and selectively endocytosed by Hc7 cells (Fig. 5). After subsequent liposomal degradation and release of the quenched fluorophores, dequenching results in intense intracellular CF fluorescence. Endocytosis of immunoliposomes bearing trastuzumab Fab' fragments clearly depends on cellular HER2 expression: MCF7 and CV1 cells, which have physiological or no HER2 expression, respectively, take up immunoliposomes either very feebly or not at all, and do not show robust intracellular fluorescence.

As vehicles for delivering fluorescent and EPR imaging agents to tumor cells, immunoliposomes have inherent

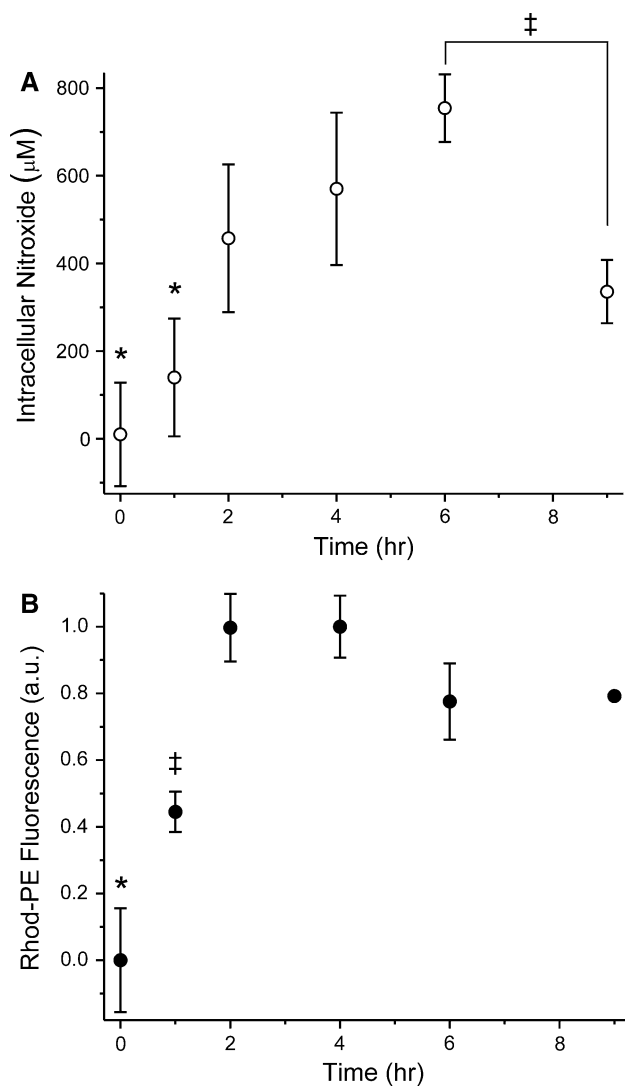


Fig. 6 Hc7 cellular uptake of Rhod-PE-containing immunoliposomes encapsulating nitroxide. Dishes of Hc7 cells were incubated at 37°C with immunoliposomes containing Rhod-PE and loaded with nitroxide **1**. At various times, intracellular nitroxide (**a**) and Rhod-PE (**b**) were assayed spectroscopically ($n = 3$). By 6 h, intracellular nitroxide had increased to $\sim 750 \mu\text{M}$ through immunoliposomal endocytosis, as verified by parallel uptake of liposomal Rhod-PE. Beyond 6 h, endocytosis slowed markedly (evidenced by lack of further Rhod-PE accumulation) and intracellular nitroxide signal declined (error bars represent SD; where not seen, the bar was smaller than the symbol). Statistical significance ($P < 0.05$) is denoted by asterisks and double-daggers. ANOVA values: panel **a**, $F_{5,17} = 11.49$; panel **b**, $F_{5,17} = 53.79$

advantages. Because the liposomes encapsulate imaging probes at self-quenching concentrations, they are spectroscopically “dark” (see Supplemental Fig. S2; [14]). This minimizes background signal from unendocytosed liposomes. After endocytosis, release and dilution of the encapsulated probes into the cell dequenches the probe signal, causing the cell to become spectroscopically “bright”. Moreover, in contrast to targeting mechanisms

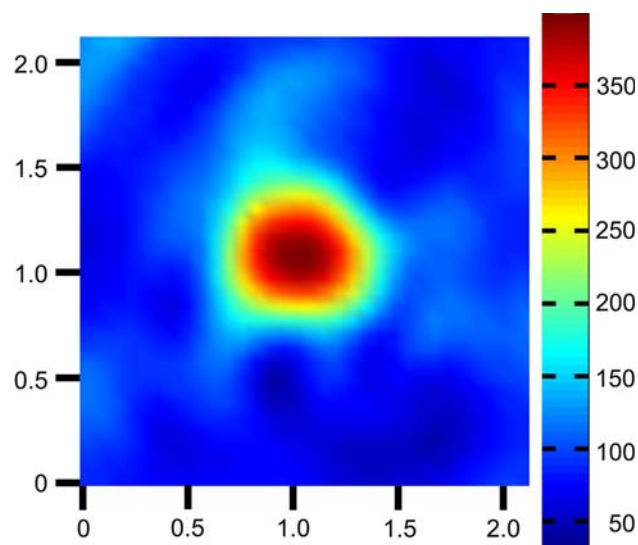


Fig. 7 EPR image of nitroxide-impregnated agarose phantom. End view of an agarose cylinder containing $100 \mu\text{M}$ nitroxide **2**. The cylinder is 6 mm in diameter and 3 mm in length. Cross-sectional view shown is from the approximate center of the cylinder’s axial dimension. The known geometry of the cylinder is well represented in the image. Signal from the cylinder is imaged with a signal-to-noise ratio of 79 and a spatial resolution of 4.4 mm. All axis labels are in centimeters and spectral intensity is encoded according to the scale shown on the right

where an antibody is directly labeled with molecular probes, immunoliposomes efficiently deliver high levels of imaging agents to cells for improved SNR in imaging. For example, each endocytosed liposome with an outer diameter of 100 nm and encapsulating 150 mM molecular probes delivers $\sim 34,000$ probe molecules. The consequent signal amplification is essential for EPRI. Immunoliposome uptake enabled Hc7 cells to accumulate nitroxide intracellularly at $\sim 750 \mu\text{M}$ (Fig. 6), which is ample for EPRI with high SNR (Fig. 7).

Using immunoliposomes to deliver nitroxides to HER2-overexpressing tumors in vivo requires additional considerations. First, liposomes are cleared from circulation by the reticulo-endothelial system (RES) [32], and must be engineered to evade such clearance. Incorporating into the liposomes a small proportion of lipid conjugated to poly(ethyleneglycol) (PEG) retards clearance by the RES [33]. The longer circulation times of such sterically stabilized, “PEGylated” liposomes enhance their targeting potential in vivo. Second, liposome delivery to tumor cells depends on tumor vascularization. While a previous study of immunoliposomes in a xenograft model suggests relatively uniform micro-distribution within tumors [34], the macro-distribution could be inhomogeneous owing to differential vascularization. Because liposomes may access only a fraction of the tumor volume, despite the very high intracellular concentrations potentially achievable with

immunoliposomal delivery, the total nitroxide content of the entire tumor may still be modest. This motivates additional innovations to enhance SNR.

SNR in EPRI can be improved by delivering more nitroxide molecules to cells, and by optimizing the spectroscopic properties of the molecules themselves. Although larger liposomes can encapsulate more nitroxide, liposomes with 100-nm outer diameter are already near-optimal *in vivo*. Increasing the diameter leads to increased circulatory clearance and reduced extravasation, both of which offset the advantage of the larger luminal volume [35, 36]. Fortunately, the performance of nitroxides as EPR imaging agents can be improved through rational design. First, we can synthesize nitroxides that are zwitterionic at physiologic pH. Such nitroxides would be highly water-soluble but would require no counter ions, which normally increase the osmolarity of the encapsulated solution but contribute no imageable signal. Zwitterionic nitroxides can be encapsulated at 300 mM—twice the concentration of nitroxide **1**, which is a mono-anion at physiological pH. Second, we can synthesize deuterium- and ¹⁵N-substituted nitroxides, which have narrower spectral peaks and correspondingly larger peak amplitudes. Preliminary studies indicate that for nitroxide **2**, isotopic substitution increases the EPR peak amplitude by close to 10-fold (unpublished observations). These two improvements should significantly enhance the feasibility of visualizing Hc7 tumors *in vivo* by EPR imaging.

EPRI is an emergent imaging modality that could offer sensitive detection of HER2-overexpressing tumors, and useful insight into their physiology. The demonstration that it is possible to use anti-HER2 immunoliposomes to deliver high concentrations of nitroxides selectively to HER2-overexpressing tumor cells bodes well for high-contrast EPRI of HER2-overexpressing tumors. Current efforts are aimed at developing Hc7 xenograft models, increasing persistence of immunoliposomes in circulation, and optimizing nitroxide molecular structure for EPRI.

Acknowledgments The authors wish to thank Drs. Brian M. Hagen and Andrew P. Ziman (University of Maryland Biotechnology Institute and University of Maryland, Baltimore) for assistance with confocal microscopy image acquisition and analysis. This work was supported by National Institutes of Health Grants GM-56481 (J. P. Y. Kao), P41-EB-2034 (G. M. Rosen and H. J. Halpern), CA-98575 (H. J. Halpern), CA124704-03 (S. S. Martin), and CA-027440 (A. M. Brodie).

References

- Alix-Panabieres C, Muller V, Pantel K (2007) Current status in human breast cancer micrometastasis. *Curr Opin Oncol* 19:558–563. doi:10.1097/CCO.0b013e3282f0ad79
- Park D, Karesen R, Naume B et al (2009) The prognostic impact of occult nodal metastasis in early breast carcinoma. *Breast Cancer Res Treat*. doi: 10.1007/s10549-009-0340-2
- Naumov GN, Townson JL, MacDonald IC et al (2003) Ineffectiveness of doxorubicin treatment on solitary dormant mammary carcinoma cells or late-developing metastases. *Breast Cancer Res Treat* 82:199–206. doi:10.1023/B:BREA.0000004377.12288.3c
- Halpern HJ, Spencer DP, Vanpolen J et al (1989) Imaging radio-frequency electron-spin-resonance spectrometer with high-resolution and sensitivity for *in vivo* measurements. *Rev Sci Instrum* 60:1040–1050
- Carrington A, McLachlan A (1967) Introduction to magnetic resonance. Harper & Row, New York, pp 1–4
- Elas M, Ahn KH, Parasca A et al (2006) Electron paramagnetic resonance oxygen images correlate spatially and quantitatively with Oxylite oxygen measurements. *Clin Cancer Res* 12:4209–4217
- Elas M, Bell R, Hleihel D et al (2008) Electron paramagnetic resonance oxygen image hypoxic fraction plus radiation dose strongly correlates with tumor cure in FSa fibrosarcomas. *Int J Radiat Oncol Biol Phys* 71:542–549
- Halpern HJ, Chandramouli GV, Barth ED et al (1999) Diminished aqueous microviscosity of tumors in murine models measured with *in vivo* radiofrequency electron paramagnetic resonance. *Cancer Res* 59:5836–5841
- Khramtsov VV, Weiner LM, Grigoriev IA et al (1982) Proton exchange in stable nitroxyl radicals. EPR study of the pH of aqueous solutions. *Chem Phys Lett* 91:69–72
- Dreher MR, Elas M, Ichikawa K et al (2004) Nitroxide conjugate of a thermally responsive elastin-like polypeptide for noninvasive thermometry. *Med Phys* 31:2755–2762
- Utsumi H, Yamada K, Ichikawa K et al (2006) Simultaneous molecular imaging of redox reactions monitored by Overhauser-enhanced MRI with 14 N- and 15 N-labeled nitroxyl radicals. *Proc Natl Acad Sci USA* 103:1463–1468
- Rosen GM, Burks SR, Kohr MJ et al (2005) Synthesis and biological testing of aminoxyls designed for long-term retention by living cells. *Org Biomol Chem* 3:645–648. doi:10.1039/b415586f
- Kao JP, Barth ED, Burks SR et al (2007) Very-low-frequency electron paramagnetic resonance (EPR) imaging of nitroxide-loaded cells. *Magn Reson Med* 58:850–854. doi:10.1002/mrm.21388
- Burks SR, Barth ED, Halpern HJ et al (2009) Cellular uptake of electron paramagnetic resonance imaging probes through endocytosis of liposomes. *Biochim Biophys Acta* 1788:2301–2308. doi:10.1016/j.bbame.2009.08.007
- Park JW, Kirpotin DB, Hong K et al (2001) Tumor targeting using anti-her2 immunoliposomes. *J Control Release* 74:95–113. doi:S0168365901003157
- Park JW, Hong K, Kirpotin DB et al (2002) Anti-HER2 immunoliposomes: enhanced efficacy attributable to targeted delivery. *Clin Cancer Res* 8:1172–1181
- King CR, Kraus MH, Aaronson SA (1985) Amplification of a novel *v-erbB*-related gene in a human mammary carcinoma. *Science* 229:974–976
- Shepard HM, Lewis GD, Sarup JC et al (1991) Monoclonal antibody therapy of human cancer: taking the HER2 protooncogene to the clinic. *J Clin Immunol* 11:117–127
- Kraus MH, Popescu NC, Amsbaugh SC et al (1987) Overexpression of the EGF receptor-related proto-oncogene *erbB-2* in human mammary tumor cell lines by different molecular mechanisms. *EMBO J* 6:605–610
- Slamon DJ, Clark GM, Wong SG et al (1987) Human breast cancer: correlation of relapse and survival with amplification of the *HER-2/neu* oncogene. *Science* 235:177–182
- Marx D, Schauer A, Reiche C et al (1990) *c-erbB2* expression in correlation to other biological parameters of breast cancer. *J Cancer Res Clin Oncol* 116:15–20

22. Schmitz KR, Ferguson KM (2009) Interaction of antibodies with ErbB receptor extracellular regions. *Exp Cell Res* 315:659–670. doi:[10.1016/j.yexcr.2008.10.008](https://doi.org/10.1016/j.yexcr.2008.10.008)
23. Baselga J, Albanell J, Molina MA et al (2001) Mechanism of action of trastuzumab and scientific update. *Semin Oncol* 28:4–11. doi:[10.1053/seon.2001.28004](https://doi.org/10.1053/seon.2001.28004)
24. Sliwkowski MX, Lofgren JA, Lewis GD et al (1999) Nonclinical studies addressing the mechanism of action of trastuzumab (Herceptin). *Semin Oncol* 26:60–70
25. Yarden Y (2001) Biology of HER2 and its importance in breast cancer. *Oncology* 61(Suppl 2):1–13. doi:[10.1007/s12094-001-0001-1](https://doi.org/10.1007/s12094-001-0001-1)
26. Ogawa M, Kosaka N, Choyke PL et al (2009) In vivo molecular imaging of cancer with a quenching near-infrared fluorescent probe using conjugates of monoclonal antibodies and indocyanine green. *Cancer Res* 69:1268–1272. doi:[10.1158/0008-5472.CAN-08-3116](https://doi.org/10.1158/0008-5472.CAN-08-3116)
27. Orlova A, Wallberg H, Stone-Elander S et al (2009) On the selection of a tracer for PET imaging of HER2-expressing tumors: direct comparison of a ¹²⁴I-labeled affibody molecule and trastuzumab in a murine xenograft model. *J Nucl Med* 50:417–425. doi:[10.2967/jnumed.108.057919](https://doi.org/10.2967/jnumed.108.057919)
28. Chen TJ, Cheng TH, Chen CY et al (2009) Targeted Herceptin-dextran iron oxide nanoparticles for noninvasive imaging of HER2/neu receptors using MRI. *J Biol Inorg Chem* 14:253–260. doi:[10.1007/s00775-008-0445-9](https://doi.org/10.1007/s00775-008-0445-9)
29. Barrett HH (1984) The Radon transformation and its applications. In: Wolf E (ed) *Progress in optics XXI*. Elsevier, Amsterdam, pp 217–286
30. Ahn KH, Halpern HJ (2007) Simulation of 4D spectral-spatial EPR images. *J Magn Reson* 187:1–9
31. Szollosi J, Balazs M, Feuerstein BG et al (1995) ERBB-2 (HER2/neu) gene copy number, p185HER-2 overexpression, and intratumor heterogeneity in human breast cancer. *Cancer Res* 55:5400–5407
32. Liu F, Liu D (1996) Serum independent liposome uptake by mouse liver. *Biochim Biophys Acta* 1278:5–11
33. Woodle MC, Lasic DD (1992) Sterically stabilized liposomes. *BiochimBiophysActa* 1113:171–199
34. Kirpotin DB, Drummond DC, Shao Y et al (2006) Antibody targeting of long-circulating lipidic nanoparticles does not increase tumor localization but does increase internalization in animal models. *Cancer Res* 66:6732–6740. doi:[10.1158/0008-5472.CAN-05-4199](https://doi.org/10.1158/0008-5472.CAN-05-4199)
35. Allen TM, Cheng WW, Hare JJ et al (2006) Pharmacokinetics and pharmacodynamics of lipidic nano-particles in cancer. *Anticancer Agents Med Chem* 6:513–523
36. Charrois GJ, Allen TM (2003) Rate of biodistribution of STEALTH liposomes to tumor and skin: influence of liposome diameter and implications for toxicity and therapeutic activity. *Biochim Biophys Acta* 1609:102–108. doi:[S0005273602006612](https://doi.org/10.1016/S0005273602006612)